

Brachistochronic Non-Adiabatic Holonomic Quantum Control

Bao-Jie Liu,¹ Zheng-Yuan Xue,^{2,*} and Man-Hong Yung^{1,3,4,5,†}

¹Department of Physics, Southern University of Science and Technology, Shenzhen 518055, China

²Guangdong Provincial Key Laboratory of Quantum Engineering and Quantum Materials, and School of Physics and Telecommunication Engineering, South China Normal University, Guangzhou 510006, China

³Shenzhen Institute for Quantum Science and Engineering,

Southern University of Science and Technology, Shenzhen 518055, China

⁴Guangdong Provincial Key Laboratory of Quantum Science and Engineering, Southern University of Science and Technology, Shenzhen 518055, China

⁵Shenzhen Key Laboratory of Quantum Science and Engineering, Southern University of Science and Technology, Shenzhen, 518055, China

(Dated: October 8, 2022)

In quantum control, geometrical operations could provide an extra layer of robustness against control errors. However, the conventional non-adiabatic holonomic quantum computation (NHQC) is limited by the fact that all of the operations require exactly the same amount of evolution time, even for a small-angle rotation. Furthermore, NHQC confines the driving part of the Hamiltonian to strictly cover a fixed pulse area, making it sensitive to control errors. Here we present an unconventional approach of NHQC, termed brachistochronic NHQC, for bypassing these limitations. Specifically, with B-NHQC, non-Abelian geometric gates can be time-optimized by following the brachistochrone curve, minimizing the impact from the environmental decoherence. Additionally, we demonstrate that B-NHQC is compatible with composed pulses, which can further enhance the robustness against pulse errors. For benchmarking, we provide a thorough analysis on the performance of B-NHQC under experimental conditions; we found that the gate error can be reduced by as much as 64% compared with NHQC.

Introduction.— Realizing precise and noise-resistant quantum gates are of vital importance to the success of quantum computation. Geometric phases, depending only on the global properties of the evolution paths, are immune to local errors [1–3]. Therefore, geometric quantum computation [4–9], where quantum gates are induced by geometric phases, is a promising strategy for fault-tolerant quantum computation. In fact, a geometric phase can either be a real number (Abelian), also known as “Berry’s phase” [10], or a matrix (non-Abelian) [11], which is the key ingredient in constructing quantum operations for holonomic quantum computation.

Holonomic quantum computation based on adiabatic evolution has been proposed [12, 13]. However, the adiabatic condition implies a lengthy gate time, thus the environment-induced decoherence would introduce severe gate infidelity. To overcome this problem, nonadiabatic holonomic quantum computation (NHQC) have been proposed to remove the adiabatic condition [17, 18]. Moreover, NHQC can be extended to realize arbitrary single-qubit holonomic quantum gate in a single-loop/shot evolution [19–24] and compatible with elementary optimal control techniques [25–27]. Recently, elementary holonomic quantum gates have been experimentally demonstrated in different platforms, including superconducting circuits [28–31], nuclear magnetic resonance (NMR) [32–34], and nitrogen-vacancy centers in diamond [35–40], etc. However, these NHQC implementations are sensitive to systematic errors due to the stringent requirements on the govern Hamiltonian [41–45].

Here, we present an unconventional approach of NHQC, called B-NHQC, for breaking the two limitations of the conventional NHQC, which extends the unconventional Abelian geometric scheme [46, 47] the non-Abelian case. Comparing with previous implementations of conventional NHQC,

our scheme is more robust against control induced imperfections, as the fixed pulse area limitation is removed. Moreover, we can combine our model with various composite-pulse schemes to further enhance the robustness of B-NHQC. Furthermore, our scheme also incorporates with the time-optimal technology [48–51], by solving the quantum brachistochrone equation (QBE), to realize universal holonomic gates with *minimum* time, and thus minimizes the decoherence induced gate infidelity. For demonstration, we consider a three-level quantum system to explain the working mechanism of B-NHQC. Numerical simulations indicate that our B-NHQC and its’ optimization can achieve a significant improvement over the NHQC gates [17, 18] using experimental parameters.

General model.— We consider a general time-dependent Hamiltonian $H(t)$. Assume $\{|\psi_m(t)\rangle\}$ is a complete set of basis, the vectors of which, at each moment of time t , follow the time-dependent Schrödinger equation (TDSE), i.e., $i|\dot{\psi}_k(t)\rangle = H(t)|\psi_k(t)\rangle$, and thus the time evolution operator $U(t, 0) = \mathcal{T}e^{-i\int_0^t H(t')dt'} = \sum_m |\psi_m(t)\rangle \langle\psi_m(0)|$. Meanwhile, we can set a different set of time-dependent basis, $\{|\phi_k(t)\rangle\}$, which satisfies the boundary conditions at time $t = 0$ and $t = \tau$, $|\phi_k(\tau)\rangle = |\phi_k(0)\rangle = |\psi_k(0)\rangle$. By aid of $|\phi_k(t)\rangle$, we can always write, $|\psi_m(t)\rangle = \sum_k V_{mk}(t) |\phi_k(t)\rangle$. Substituting the solutions into TDSE and applying the boundary conditions, we obtain the following unitary transformation matrix at the final time $t = \tau$ as $U(\tau) = \sum_{ml} [\mathbf{T}e^{i(\mathbf{A}+\mathbf{K})}]_{ml} |\psi_m(0)\rangle \langle\psi_l(0)|$, where \mathbf{T} is time ordering operator, the dynamical and geometric parts are denoted by $K_{ml} \equiv -\int_0^\tau \langle\phi_m(t)| H(t) |\phi_l(t)\rangle dt$ and $A_{ml} \equiv \int_0^\tau i \langle\phi_m(t)| \frac{d}{dt} |\phi_l(t)\rangle dt$.

Here, we extend the definition the unconventional geometric phase [46, 47] from the Abelian case to a non-Abelian

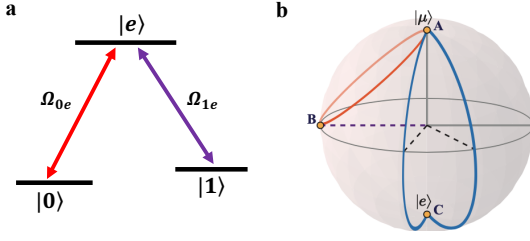


FIG. 1. Illustration of the proposed scheme. (a) The coupling configuration with two microwave fields Ω_{0e} and Ω_{1e} resonantly coupled to the three levels of a quantum system. (b) Geometric illustration of the proposed B-NHQC gate on the Bloch sphere, where the state $|\mu\rangle$ undergoes a cyclic evolution $A \rightarrow B \rightarrow A$. However, the conventional NHQC takes a cyclic evolution $A \rightarrow C \rightarrow A$.

holonomic case, where the generalized unconventional quantum holonomy satisfies

$$\mathbf{K} = \eta \mathbf{A} + \mathbf{G}, \quad (1)$$

where η is a proportional constant and the matrix \mathbf{G} depends only on the global geometric feature of the evolution path. Hence, we obtain our target unconventional holonomy in the $\{|\psi_m\rangle\}$ basis as

$$U(\tau) = \mathbf{T}e^{i[(1+\eta)\mathbf{A}+\mathbf{G}]}. \quad (2)$$

Inevitably, any implementation will suffer from decoherence, which reduces the target gate fidelity, and thus operations with *minimum* time becomes a preferable choice for realizing high-fidelity gates. To realize the fastest geometric gates, we extend the above framework to B-NHQC, by combining it with the time-optimal control technique [48–51], via solving the QBE

$$i\partial F/\partial t = [H, F], \quad (3)$$

where $F = \partial L_c/\partial H$ and $L_c = \sum_j \mu_j f_j(H)$, with μ_j being the Lagrange multiplier. Note that, choosing different parameters of the driven Hamiltonian $H(t)$ makes the evolution of the system follow different paths, but leads to a same unconventional holonomic gate. The path with the minimal time can be obtained by solving the QBE together with TDSE. For a realistic physical systems, there always be a constraint that the energy bandwidth, described by $f_0(H) = [Tr(H^2) - E^2]/2$, should be finite.

Application of B-NHQC.— We firstly illustrate the implementation of our idea in a three-level system, where the ground state $|0\rangle$ and $|1\rangle$ are chosen as logic states of the qubit, while the excited state $|e\rangle$ as an auxiliary state, as shown in Fig. 1(a). The transitions of $|0\rangle \leftrightarrow |e\rangle$ and $|e\rangle \leftrightarrow |1\rangle$ are driven resonantly by two microwave fields, with the amplitudes $\Omega_{0e}(t)$, $\Omega_{e1}(t)$ and the phases ϕ_0 and $\phi(t)$, respectively. Assuming $\hbar = 1$ hereafter, the Hamiltonian of the system is

$$H_1(t) = \frac{\Omega(t)}{2} e^{i\phi(t)} \left(\sin \frac{\theta}{2} e^{i\phi_1} |0\rangle + \cos \frac{\theta}{2} |1\rangle \right) \langle e| + \text{H.c.}, \quad (4)$$

where $\phi_1 = \phi_0 - \phi(t)$, $\Omega(t) = \sqrt{\Omega_{0e}^2(t) + \Omega_{1e}^2(t)}$ and $\tan(\theta/2) = \Omega_{0e}(t)/\Omega_{1e}(t)$, and the mixing angle θ is set to be time-independent for simplicity.

As a set of orthogonal solutions of TDSE $\{|\psi_m(t)\rangle\}$ can be parameterized with two angles $\chi(t)$, $\alpha(t)$, and a global phase $\zeta(t)$ as

$$\begin{aligned} |\psi_0(t)\rangle &= e^{-i\zeta(t)} \left(\sin \frac{\chi}{2} e^{-i\frac{\alpha(t)}{2}} |\mu\rangle + \cos \frac{\chi}{2} e^{i\frac{\alpha(t)}{2}} |e\rangle \right), \\ |\psi_1(t)\rangle &= e^{i\frac{\zeta(t)}{2}} \left(\cos \frac{\chi}{2} e^{-i\frac{\alpha(t)}{2}} |\mu\rangle - \sin \frac{\chi}{2} e^{i\frac{\alpha(t)}{2}} |e\rangle \right), \\ |\psi_2(t)\rangle &= \cos(\theta/2) |0\rangle + \sin(\theta/2) e^{-i\phi_1} |1\rangle, \end{aligned} \quad (5)$$

with $|\mu_0\rangle = \sin(\theta/2) e^{i\phi_1} |0\rangle + \cos(\theta/2) |1\rangle$. Taking $H_1(t)$ in Eq. (4) and $|\psi_m(t)\rangle$ into TDSE, we obtain

$$\begin{aligned} \dot{\chi}(t) &= \Omega(t) \sin[\phi(t) - \alpha(t)], \\ \dot{\alpha}(t) &= -\cot \chi(t) \Omega(t) \cos[\phi(t) - \alpha(t)], \\ \dot{\zeta}(t) &= \dot{\alpha}(t) \cos \chi(t) - \Omega \cos[\phi(t) - \alpha(t)] \sin \chi(t). \end{aligned} \quad (6)$$

Therefore, the evolution operator is obtained as $U(t) = \mathcal{T}e^{-i\int_0^t H_1(t') dt'} = \sum_{m=0}^{m=2} |\psi_m(t)\rangle \langle \psi_m(0)|$.

To construct the holonomic gate, we choose a set of auxiliary states as $|\phi_1(t)\rangle = e^{i\gamma} [\sin \frac{\chi}{2} |\psi_0(t)\rangle + \cos \frac{\chi}{2} |\psi_1(t)\rangle]$ and $|\phi_2(t)\rangle = |\psi_2(t)\rangle$, satisfying the boundary conditions $|\phi_1(0)\rangle = |\phi_1(\tau)\rangle = |\mu\rangle$. When the cyclic evolution condition $\zeta(\tau) = 2\pi$ is met with the path $A \rightarrow B \rightarrow A$ shown in Fig. 1(b), the unconventional holonomic unitary matrix in Eq. (1) on computational subspace $\{|\phi_1(0)\rangle, |\phi_2(0)\rangle\}$ is

$$U(\tau) = e^{i\mathbf{G}} = \begin{pmatrix} e^{i\gamma} & 0 \\ 0 & 1 \end{pmatrix}, \quad (7)$$

where the control parameters $\dot{\chi} = 0$ and $\alpha = \phi$ are chosen. Meanwhile, $\mathbf{A} = \begin{pmatrix} \gamma - \int_0^\tau \Omega \sin \chi \cos \chi \sin^2 \zeta dt & 0 \\ 0 & 0 \end{pmatrix}$, $\eta = -1$, and $\gamma = \pi - \alpha(\tau)/2$. Note that Eq. (7) is a holonomy associated with a closed smooth C in the base space of Grassmann manifold $G(3, 2)$, which is the set of two-dimensional computational subspaces within the Hilbert space spanned by the state vectors $\{|0\rangle, |1\rangle, |e\rangle\}$.

In the logical qubit subspace $\{|0\rangle, |1\rangle\}$, $U(\tau)$ leads to a unconventional holonomic single-qubit gate of

$$U(\theta, \phi_1, \gamma) = \exp\left(i\frac{\gamma}{2}\right) \exp\left(-i\frac{\gamma}{2} \mathbf{n} \cdot \boldsymbol{\sigma}\right), \quad (8)$$

which describes a rotation around the $\mathbf{n} = (\sin \theta \cos \phi, \sin \theta \sin \phi, \cos \theta)$ axis by a γ angle. Since \mathbf{n} and γ can be arbitrary, $U(\theta, \phi_1, \gamma)$ can construct arbitrary single-qubit gates, in a single loop evolution. Moreover, our scheme can reduce to the conventional NHQC scheme [17, 18], simply by setting $\chi = \pi/2$ and $\alpha = 0$. Then, the evolution satisfies the parallel transport condition, i.e., $\gamma_d = 0$, and the unconventional geometric phase $\gamma = \pi$ becomes a pure geometric phase.

Recall that for realizing B-NHQC gates, we need to minimize the above gate time by solving the QBE in Eq. (3) to reduce the influence of the decoherence effect. Here, we can

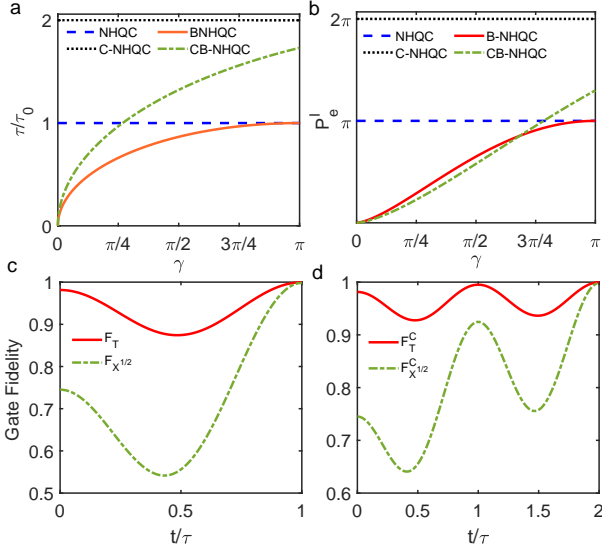


FIG. 2. (a) The dimensionless gate time and (b) the integrated excited-state population P_e^I of B-NHQC, CB-NHQC, NHQC and C-NHQC schemes with respect to the rotation angle γ . Dynamics of gate fidelities of $X^{1/2}$ and T gates in B-NHQC (c) and CB-NHQC (d) schemes.

simply set $\Omega(t) = \Omega_0$ to satisfy the constraint, i.e., $f_0(H_1) = [\text{Tr}(H_1^2) - \Omega_0^2]/2 = 0$. Following the Ref. [50, 51], by solving the Eq. (3), one minimum-time solution to our purpose is $\phi(t) = \alpha(t) = 2(\gamma - \pi)t/\pi\tau$, with the minimum evolution time being $\tau = 2\sqrt{\pi^2 - (\pi - \gamma)^2}/\Omega_0$, which decreases with the decrease of the geometric phase γ .

Furthermore, we can enhance the robustness of B-NHQC against systematic control errors by combining it with the composite pulse strategy, which we call CB-NHQC, similar to the case of composite NHQC (C-NHQC) [34, 53]. To achieve this, the CB-NHQC is divided into two parts, i.e., $(0, \tau)$ and $(\tau, 2\tau)$. During the first interval $(0 \leq t \leq \tau)$, we set the phase $\phi(t) = 2(\gamma/2 - \pi)t/\tau$ corresponding to the evolution operator $U_1(\theta, \phi_1, \gamma/2)$. For the second interval, $\phi'(t) = \pi + 2(\gamma/2 - \pi)t/\pi\tau$ with the evolution operator $U_2 = -U_1$. As a result, the obtained CB-NHQC gate is

$$U_C(\theta, \phi_1, \gamma) = -[U_1(\theta, \phi_1, \gamma/2)]^2. \quad (9)$$

Here, we plot the evolution time τ , in unit of $\tau_0 = 2\pi/\Omega_0$, of B-NHQC, CB-NHQC, NHQC and C-NHQC as a function of their corresponding geometric phases, as shown in Fig. 2(a), which clearly shows that B-NHQC scheme generally has a shortest gate time comparing with other schemes. Moreover, as shown in Fig. 2(b), B-NHQC and CB-NHQC schemes can greatly reduce the integrated excited-state populations $P_e^I = \int_0^\tau |\langle \psi(t) | e \rangle|^2 dt$ compared with NHQC and C-NHQC corresponding to the initial state $|\mu\rangle$, which are beneficial to reduce the excited-state decay.

The performance of our proposal in Eq. (8) can be evalu-

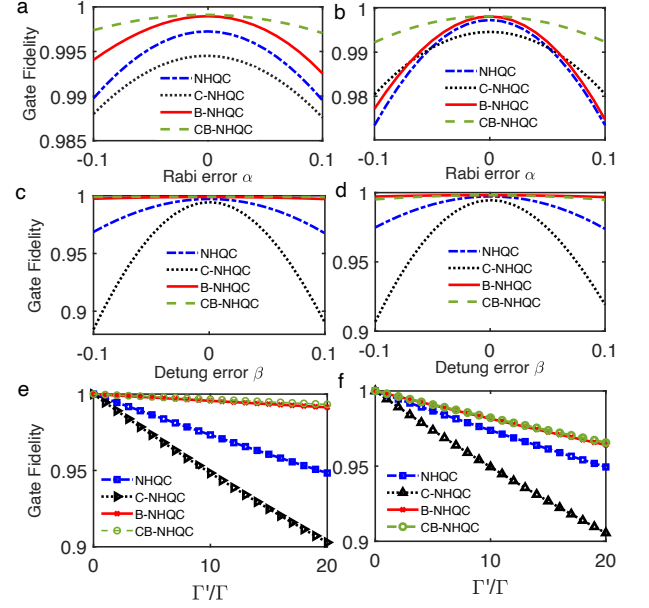


FIG. 3. The gate fidelities under imperfections. The T and $X^{1/2}$ gate fidelities for B-NHQC, CB-NHQC, NHQC and C-NHQC cases under the Rabi error (a) and (b), detuning error (c) and (d), decoherence (e) and (f), respectively.

ated by using the quantum master equation of

$$\dot{\rho}_1 = i[\rho_1, H_1] + \frac{\Gamma_-}{2}\mathcal{L}(S_-) + \frac{\Gamma_z}{2}\mathcal{L}(S_z), \quad (10)$$

where ρ_1 is the density matrix of the considered system, $\mathcal{L}(A) = 2A\rho_1 A^\dagger - A^\dagger A\rho_1 - \rho_1 A^\dagger A$ is the Lindbladian of the operator of A , $S_- = |0\rangle\langle e| + |1\rangle\langle e|$ and $S_z = |e\rangle\langle e| - |1\rangle\langle 1| - |0\rangle\langle 0|$, Γ_- and Γ_z are the decay and dephasing rates of the transmon, respectively. In our simulation, we choose the parameters from the current experiment [52] as $\Gamma_- = \Gamma_z = \Gamma = \Omega_0/2000$. We evaluate the T gate $U_T = U(0, 0, \pi/4)$ and the $X^{1/2}$ gate $U_{X^{1/2}} = U(\pi/2, 0, \pi/2)$, using the gate fidelity defined by $F_{T, X^{1/2}} = \frac{1}{2\pi} \int_0^{2\pi} \langle \psi_{T, X^{1/2}} | \rho_1 | \psi_{T, X^{1/2}} \rangle d\chi_1$ for a general initial state of $|\psi(0)\rangle = \cos \chi_1 |0\rangle + \sin \chi_1 |1\rangle$ with the target state being $|\psi_{T, X^{1/2}}\rangle = U_{T, X^{1/2}} |\psi\rangle$. As show in Figs. 2(c) and 2(d), we plot gate fidelities as functions of the time τ for 1001 input states with χ_1 uniformly distributed over $[0, 2\pi]$, and the obtained T gate and $X^{1/2}$ fidelities in B-NHQC are $F_{X^{1/2}} = 99.81\%$ and $F_T = 99.90\%$, and $F_{X^{1/2}}^C = 99.82\%$ and $F_T^C = 99.92\%$ in CB-NHQC.

Robustness.— We now proceed to show the robustness improvement of our scheme. Firstly, to investigate the robustness against pulse errors, we assume the amplitudes of driven pulse to vary in the range of $(1 + \alpha)\Omega_0$ with the error fraction $\alpha \in [-0.1, 0.1]$. Secondly, we set the frequency detuning error to be $\Delta|e\rangle\langle e|$ with $\Delta = \beta\Omega_0$ being static and the fraction is $\beta \in [-0.1, 0.1]$. As show Figs. 3, we plot the T (3a) and $X^{1/2}$ (3b) gate fidelities of B-NHQC, CB-NHQC, NHQC and C-NHQC as functions of the error fraction α and β with the relaxation, and find our CB-NHQC strategy is indeed the most robust than the other schemes against both Rabi errors

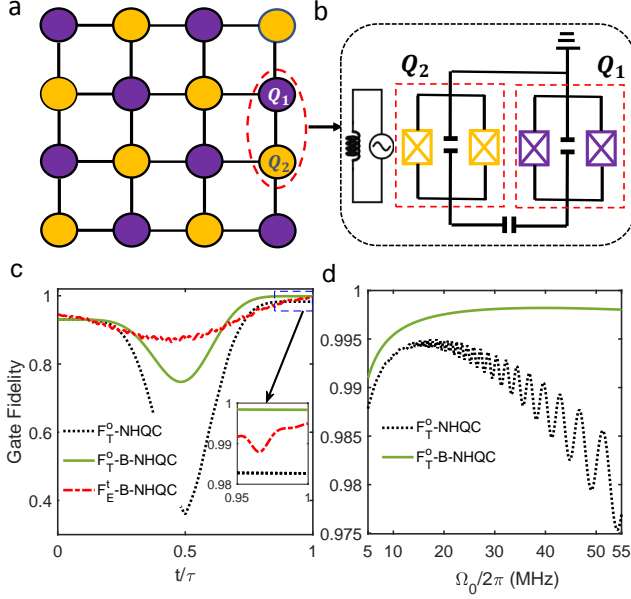


FIG. 4. (a) Scale-up of our physical scheme, the 2D square qubit lattice includes capacitively coupled superconducting transmon qubits, where the transmon qubits are denoted by filled circles. (b) Schematic of our circuit consisting of two capacitively coupled qubits, where Q_2 is biased by an ac magnetic flux to periodically modulate its transition frequency. (c) The T and two-qubit entangled gate fidelities of B-NHQC as a function of the time. (d) The gate fidelities of the B-NHQC and NHQC geometric T gates as functions of the tunable parameters Ω_0 .

and detuning errors. Thirdly, we also plot the T and $X^{1/2}$ gate fidelities as a function of decoherence rate Γ for all the four schemes. As shown in Fig. 3(e) and 3(f), our schemes of B-NHQC and CB-NHQC can greatly suppress the decoherence effect comparing with NHQC and C-NHQC.

Physical realization on superconducting circuits.—Here, we illustrate the implementation of our idea on superconducting circuits, as shown in Figs. 4(a) and 4(b). We consider the three lowest levels of a transmon qubit, where the state $|g\rangle \equiv |0\rangle$ and the state $|f\rangle \equiv |1\rangle$ are chosen as our qubit logic states; while the state $|e\rangle$ as an auxiliary state, the third excited state $|h\rangle \equiv |2\rangle$ as a leakage state. The corresponding Hamiltonian, in the interaction picture, is approximately given by Eq. (4). Thus, we can realize B-NHQC single-qubit gate in a single-loop way with a superconducting transmon device.

In our simulation, we choose the simple pulse $\Omega(t) = \Omega_0 \sin^2(\pi t/\tau)$ to suppress the cross coupling and leakage to higher excited energy levels due to the intrinsic weak anharmonicity κ of the transmon qubit. Using the parameters in current experiments [55, 56], $\Omega_0 = 2\pi \times 45$ MHz, $\Gamma = 2\pi \times 4$ kHz, and $\kappa = -2\pi \times 260$ MHz, we found that the single-qubit T gate fidelity F_T^0 can be significantly improved from 98.40% to 99.84% compared with NHQC under the same experimental conditions, and the minimum gate error can be reduced by as much as 64% compared with NHQC, as shown in Fig. 4(c) and 4(d).

Nontrivial two-qubit gates can be implemented on two capacitively coupled transmons, denoting as Q_1 and Q_2 , as shown in Fig. 4(b). The Hamiltonian can be written as $H_{\text{sys}} = \sum_{k=1}^2 H_{q_k} + H_{q_c}$ where H_{q_k} is the single-qubit Hamiltonian and H_{q_c} is the coupling term. With the lowest four levels of a transmon being considered, the free single-qubit Hamiltonian is $H_{q_k} = \omega_{q_k} |e\rangle \langle e| + (2\omega_{q_k} + \kappa_k) |1\rangle \langle 1| + (3\omega_{q_k} + 2\kappa_k) |2\rangle \langle 2|$, where ω_{q_k} is the resonant frequency of a transmon, κ_k is the corresponding anharmonicity. Meanwhile, the two-qubit coupling Hamiltonian is $H_{q_c} = g_{12} (\sigma_1^\dagger \otimes \sigma_2 + \text{H.c.})$, where g_{12} is the static capacitive coupling strength, and $\sigma_i = |0\rangle \langle e| + \sqrt{2}|e\rangle \langle 1| + \sqrt{3}|1\rangle \langle 2|$ is the lower operator for the transmon. To obtain tunable coupling between the two qubits, we add an ac magnetic flux on transmon Q_2 to periodically modulate its eigen-frequency as $\omega_{q_2}(t) = \omega_{q_2} + \varepsilon \sin(\nu t)$, where ε and ν are the modulation amplitude and frequency, respectively. Moving into the interaction picture, the interaction Hamiltonian reads [57–60]

$$H_I = g_{12} [\sqrt{2}e^{i(\Delta_1 - \kappa_2)t} e^{i\beta \cos(\nu t)} |ee\rangle \langle 01| + \sqrt{2}e^{i(\Delta_1 - \kappa_1)t} e^{i\beta \cos(\nu t)} |10\rangle \langle ee| + \sqrt{6}e^{i(\Delta_1 - \kappa_2 + 2\kappa_1)t} e^{i\beta \cos(\nu t)} |2e\rangle \langle 11| + \sqrt{6}e^{i(\Delta_1 - 2\kappa_2 + \kappa_1)t} e^{i\beta \cos(\nu t)} |11\rangle \langle e2| + \text{H.c.}], \quad (11)$$

where $\Delta_1 = \omega_1 - \omega_2$, $\beta = \varepsilon/\nu$, and $|mn\rangle \equiv |m\rangle_1 \otimes |n\rangle_2$. From the above Hamiltonian, resonant interaction can be induced in both the two or four excitation subspaces, by different choice of the driving frequency ν . Ignoring the higher-order oscillating terms, when $\Delta_1 - \kappa_2 - \mu = \nu$ with a small detuning μ , we can get the effective Hamiltonian in the subspace $\{|01\rangle, |11\rangle, |e2\rangle, |ee\rangle\}$ as,

$$H_e = \frac{1}{2} g'_{12} [e^{-i\mu t} (|ee\rangle \langle 01| + 3e^{i(\kappa_1 - \kappa_2)t} |11\rangle \langle e2|) + \text{H.c.}], \quad (12)$$

where $g'_{12} = 2\sqrt{2}g_{12}J_1(\beta)$ with $J_m(\beta)$ being the Bessel function of the first kind.

In the same way as the single-qubit phase gate case, we can realize the two-qubit entangled gate with minimum time by solving the QBE, and we obtain that $\mu = 2(\xi - \pi)/\pi$ with a minimum gate time $\tau_2 = 2\sqrt{\pi^2 - (\pi - \xi)^2}/g'_{12}$, where ξ_1 and ξ_2 corresponds to the obtained unconventional geometric phase in the subspaces $\{|01\rangle, |ee\rangle\}$ and $\{|11\rangle, |e2\rangle\}$. And the obtained evolution operator $U_E(\tau_2)$, i.e., the holonomic entangling gate ($\xi_1 \neq \xi_2$), in the two-qubit basis $\{|00\rangle, |01\rangle, |10\rangle, |11\rangle\}$ as

$$U_E(\xi_1, \xi_2) = \text{diag}(1, e^{i\xi_1}, 1, e^{i\xi_2}). \quad (13)$$

To evaluate the gate performance, we take the control T gate $U_E(\pi/4, -\pi/4)$ as a typical example. Here, we set the parameters [57, 58] of the transmons as $\kappa_1 = -2\pi \times 220$ MHz, $\kappa_2 = \kappa$, $\Delta_1 = 2\pi \times 146$ MHz and $g_{12} = 2\pi \times 10$ MHz. For a general initial state $|\psi(0)\rangle = (\cos \chi_1 |0\rangle_1 + \sin \chi_1 |1\rangle_1) \otimes (\cos \chi_2 |0\rangle_2 + \sin \chi_2 |1\rangle_2)$, the two-qubit gate fidelity defined by [60] $F_E^t = (1/4\pi^2) \int_0^{2\pi} \int_0^{2\pi} \langle \psi_{fs} | \rho_2 | \psi_{fs} \rangle d\chi_1 d\chi_2$ with

the target state $|\psi_E\rangle = U_E|\psi(0)\rangle$, the gate fidelity of U_E can be as high as 99.50%, as shown in Fig. 4(c).

Conclusion.— We have proposed an unconventional approach of NHQC scheme with non-Abelian geometric phase, which can be compatible with time-optimal control technology to realize the fastest holonomic gate. Comparing with conventional NHQC, our proposal is more robust against the experimental control errors and decoherence. We also presented an explicit way to implement our scheme using a three-level system, and numerically simulated the performance of pulse optimization for superconducting circuits, where the gate fidelity can be significantly improved. Moreover, we discuss how the B-NHQC gate presented here can be applied to two-qubit gates in detail.

We thank T. Chen for helpful discussion. This work is supported by the Key-Area Research and Development Program of Guangdong Province (Grant No. 2018B030326001), the National Natural Science Foundation of China (Grant No. 11875160 and No. 11874156), the Natural Science Foundation of Guangdong Province (Grant No. 2017B030308003), the National Key R& D Program of China (Grant No. 2016YFA0301803, the Guangdong Innovative and Entrepreneurial Research Team Program (Grant No. 2016ZT06D348), the Economy, Trade and Information Commission of Shenzhen Municipality (Grant No. 201901161512), the Science, Technology and Innovation Commission of Shenzhen Municipality (Grant No. JCYJ20170412152620376, No. JCYJ20170817105046702, and No. KYTDPT20181011104202253).

* zyxue83@163.com

† yung@sustech.edu.cn

- [1] P. Zanardi, and M. Rasetti, Phys. Lett. A **264**, 94 (1999).
- [2] E. Sjöqvist, Physics **1**, 35 (2008).
- [3] Y. Aharonov, and J. Anandan, Phys. Rev. Lett. **58**, 1593 (1987).
- [4] S.-L. Zhu, and P. Zanardi, Phys. Rev. A **72**, 020301(R) (2005).
- [5] J. A. Jones, V. Vedral, A. Ekert, and G. Castagnoli, Nature (London) **403**, 869 (2000).
- [6] S. Berger, M. Pechal, A. A. Abdumalikov, Jr., C. Eichler, L. Steffen, A. Fedorov, A. Wallraff, and S. Filipp, Phys. Rev. A **87**, 060303(R) (2013).
- [7] G. De Chiara and G. M. Palma, Phys. Rev. Lett. **91**, 090404 (2003).
- [8] P. J. Leek, J. M. Fink, A. Blais, R. Bianchetti, M. Goppl, J. M. Gambetta, D. I. Schuster, L. Frunzio, R. J. Schoelkopf, and A. Wallraff, Science **318**, 1889 (2007).
- [9] S. Filipp, J. Klepp, Y. Hasegawa, C. Plonka-Spehr, U. Schmidt, P. Geltenbort, and H. Rauch, Phys. Rev. Lett. **102**, 030404 (2009).
- [10] M. V. Berry, Proc. R. Soc. Lond. A **392**, 45 (1984).
- [11] F. Wilczek, and A. Zee, Phys. Rev. Lett. **52**, 2111 (1984).
- [12] L.-M. Duan, J. I. Cirac and P. Zoller, Science **292**, 1695 (2001).
- [13] L.-A. Wu, P. Zanardi, and D. A. Lidar, Phys. Rev. Lett. **95**, 130501 (2005).
- [14] J. Anandan, Phys. Lett. A **133**, 171 (1988).
- [15] Wang X.-B., and M. Keiji, Phys. Rev. Lett. **87**, 097901 (2001).
- [16] S.-L. Zhu, and Z. D. Wang, Phys. Rev. Lett. **89**, 097902 (2002).
- [17] E. Sjöqvist, D. M. Tong, L. M. Andersson, B. Hessmo, M. Johansson, and K. Singh, New J. Phys. **14**, 103035 (2012).
- [18] G. F. Xu, J. Zhang, D. M. Tong, E. Sjöqvist, and L. C. Kwek, Phys. Rev. Lett. **109**, 170501 (2012).
- [19] G. F. Xu, C. L. Liu, P. Z. Zhao, and D. M. Tong, Phys. Rev. A **92**, 052302 (2015).
- [20] E. Sjöqvist, Phys. Lett. A **380**, 65 (2016).
- [21] E. Herterich and E. Sjöqvist, Phys. Rev. A **94**, 052310 (2016).
- [22] P. Z. Zhao, G. F. Xu, Q. M. Ding, E. Sjöqvist, and D. M. Tong, Phys. Rev. A **95**, 062310 (2017).
- [23] G. F. Xu, D. M. Tong and E. Sjöqvist, Phys. Rev. A **98**, 052315 (2018).
- [24] Z.-P. Hong, B.-J. Liu, J.-Q. Cai, X.-D. Zhang, Y. Hu, Z. D. Wang, and Z.-Y. Xue, Phys. Rev. A **97**, 022332 (2018).
- [25] B.-J. Liu, X.-K. Song, Z.-Y. Xue, X. Wang, and M.-H. Yung, Phys. Rev. Lett. **123**, 100501 (2019).
- [26] S. Li, T. Chen, and Z.-Y. Xue, Adv. Quantum Technol. **3**, 2000001 (2020).
- [27] M.-Z. Ai, S. Li, Z. Hou, Z.-Y. Xue, J.-M. Cui, Y.-F. Huang, C.-F. Li, and G.-C. Guo, [arXiv:2006.04609](https://arxiv.org/abs/2006.04609).
- [28] A. A. Abdumalikov, J. M. Fink, K. Juliusson, M. Pechal, S. Berger, A. Wallraff, and S. Filipp, Nature (London) **496**, 482 (2013).
- [29] Y. Xu, W. Cai, Y. Ma, X. Mu, L. Hu, T. Chen, H. Wang, Y. P. Song, Z.-Y. Xue, Z.-Q. Yin, and L. Sun, Phys. Rev. Lett. **121**, 110501 (2018).
- [30] D. J. Egger, M. Ganzhorn, G. Salis, A. Fuhrer, P. Mueller, P. K. Barkoutsos, N. Moll, I. Tavernelli, and S. Filipp, Phys. Rev. Appl. **11**, 014017 (2019).
- [31] T. Yan, B.-J. Liu, K. Xu, C. Song, S. Liu, Z. Zhang, H. Deng, Z. Yan, H. Rong, M.-H. Yung, Y. Chen, and D. Yu, Phys. Rev. Lett. **122**, 080501 (2019).
- [32] G. Feng, G. Xu, and G. Long, Phys. Rev. Lett. **110**, 190501 (2013).
- [33] H. Li, Y. Liu, and G. Long, Sci. China: Phys., Mech. Astron. **60**, 080311 (2017).
- [34] Z. Zhu, T. Chen, X. Yang, J. Bian, Z.-Y. Xue, and X. Peng, Phys. Rev. Appl. **12**, 024024 (2019).
- [35] C. Zu, W.-B. Wang, L. He, W.-G. Zhang, C.-Y. Dai, F. Wang, and L.-M. Duan, Nature (London) **514**, 72 (2014).
- [36] S. Arroyo-Camejo, A. Lazarev, S. W. Hell, and G. Balasubramanian, Nat. Commun. **5**, 4870 (2014).
- [37] Y. Sekiguchi, N. Niikura, R. Kuroiwa, H. Kano, and H. Kosaka, Nat. Photonics **11**, 309 (2017).
- [38] B. B. Zhou, P. C. Jerger, V. O. Shkolnikov, F. J. Heremans, G. Burkard, and D. D. Awschalom, Phys. Rev. Lett. **119**, 140503 (2017).
- [39] N. Ishida, T. Nakamura, T. Tanaka, S. Mishima, H. Kano, R. Kuroiwa, Y. Sekiguchi, and H. Kosaka, Opt. Lett. **43**, 2380 (2018).
- [40] K. Nagata, K. Kuramitani, Y. Sekiguchi, and H. Kosaka, Nat. Commun. **9**, 3227 (2018).
- [41] J. T. Thomas, M. Lababidi, and M. Tian, Phys. Rev. A **84**, 042335 (2011).
- [42] M. Johansson, E. Sjöqvist, L. M. Andersson, M. Ericsson, B. Hessmo, K. Singh, and D. M. Tong, Phys. Rev. A **86**, 062322 (2012).
- [43] S.-B. Zheng, C.-P. Yang, and F. Nori, Phys. Rev. A **93**, 032313 (2016).
- [44] J. Jing, C.-H. Lam, and L.-A. Wu, Phys. Rev. A **95**, 012334 (2017).
- [45] N. Ramberg and E. Sjöqvist, Phys. Rev. Lett. **122**, 140501 (2019).

- [46] S.-L. Zhu and Z. D. Wang, Phys. Rev. Lett. **91**, 187902 (2003).
- [47] J. Du, P. Zou, and Z. D. Wang, Phys. Rev. A **74**, 020302 (2006).
- [48] A. Carlini and T. Koike, Phys. Rev. A **86**, 054302 (2012).
- [49] A. Carlini and T. Koike, J. Phys. A **46**, 045307 (2013).
- [50] X. Wang, M. Allegra, K. Jacobs, S. Lloyd, C. Lupo, and M. Mohseni, Phys. Rev. Lett. **114**, 170501 (2015).
- [51] J. Geng, Y. Wu, X. Wang, K. Xu, F. Shi, Y. Xie, X. Rong, and J. Du, Phys. Rev. Lett. **117**, 170501 (2016).
- [52] I. Buluta, S. Ashhab, and F. Nori, Rep. Prog. Phys. **74**, 104401 (2011).
- [53] G. F. Xu, P. Z. Zhao, T. H. Xing, E. Sjöqvist, and D. M. Tong, Phys. Rev. A **95**, 032311 (2017).
- [54] F. Motzoi, J. M. Gambetta, P. Rebentrost, and F. K. Wilhelm, Phys. Rev. Lett. **103**, 110501 (2009).
- [55] R. Barends, J. Kelly, A. Megrant, A. Veitia, D. Sank, E. Jeffrey, T. C. White, J. Mutus, A. G. Fowler, B. Campbell, *et al.*, Nature (London) **508**, 500 (2014).
- [56] Z. Chen, J. Kelly, C. Quintana, R. Barends, B. Campbell, Y. Chen, B. Chiaro, A. Dunsworth, A. G. Fowler, E. Lucero, *et al.*, Phys. Rev. Lett. **116**, 020501 (2016).
- [57] M. Reagor, C. B. Osborn, N. Tezak, A. Staley, G. Prawiroatmodjo, M. Scheer, N. Alidoust, E. A. Sete, N. Didier, M. P. da Silva, *et al.*, Sci. Adv. **4**, eaao3603 (2018).
- [58] S. A. Caldwell, N. Didier, C. A. Ryan, E. A. Sete, A. Hudson, P. Karalekas, R. Manenti, M. P. da Silva, R. Sinclair, E. Acala, *et al.*, Phys. Rev. Appl. **10**, 034050 (2018).
- [59] X. Li, Y. Ma, J. Han, T. Chen, Y. Xu, W. Cai, H. Wang, Y.P. Song, Z.-Y. Xue, Z.-Q. Yin, and L. Sun, Phys. Rev. Appl. **10**, 054009 (2018).
- [60] T. Chen and Z.-Y. Xue, Phys. Rev. Appl. **10**, 10, 054051 (2018).